Research Article

Convective Drying of Mango (*Mangifera indica* L.): Effect of Experimental Parameters on Drying Kinetics and Shrinkage

Withu Choosri[1*] and Touchpong Choosri[2]

ABSTRACT

The aims of this work were to study the effect of swirling and non-swirling air flow on drying kinetics of ripe mango and to investigate the area shrinkage of ripe mango during the drying process by computer vision system (CVS). The CVS used to evaluate the area shrinkage of dried ripe mango is a real-time monitoring method which is precise, labor-saving, non-destructive method. In particular, CVS does not disrupt an equilibrium of heat and mass transfer in the drying chamber. Ripe mangoes were dried at air temperatures of 50, 60, and 70°C and air velocities of 1.0, 1.5, and 2.0 m/s for both swirling and non-swirling air flow. The results revealed that the effective moisture diffusivity (D_{eff}), for swirling and non-swirling air flow drying, were $(4.48\text{-}9.71)\times10^{-9}$ and $(3.41\text{-}7.24)\times10^{-9}$ m^2/s, respectively. Moreover, the area shrinkage of swirling air flow drying was 32.64-40.98%, while that of non-swirling air flow drying was 36.45-43.44%. The area shrinkage of dried ripe mango was highest at low air temperature and 1.5 m/s air velocity.

Keywords: Convective drying, Swirling flow, Drying kinetic, Computer vision system, Shrinkage

[1*]Department of Food Technology, Faculty of Science, Ramkhamhaeng University, Bangkok. Thailand. 10240
[2]Department of Food Technology, Faculty of Engineering and Industrial Technology, Silpakorn University, NakonPathom, Thailand.73000
[*]Corresponding author, email: c_withu@hotmail.com

Introduction

Mangoes (*Mangifera indica* L.) are tropical fruit, which can be consumed both raw and ripe. Ripe mangoes are popular to eat for both fresh and dried (in form of drying) because of its properties such as sweet taste, pleasuring flavor, and high nutritional values. Nowadays, the consumer demand for dried fruits is high nutritional values as well as the appearance that is most similar to fresh products. On the other hand, the major problem of drying process, especially hot-air drying, is the product quality changes during the drying process due to temperature and long drying time [1].

The reduction of thermals in hot-air drying process might be able to retain and improve the quality of dried product. Using of swirling air flow is one interesting way to resolve and enhance the product qualities. In previous research, swirling air flow was used for drying in many foods, for instance, pineapple that provided 3−9% in higher drying efficiencies and lower color changes than non-swirling air flow [2]. Moreover, the former research also reported that swirling air flow was able to decrease the drying time when compared with non-swirling air flow in solar dryer [3] and fluidized bed dryer [4].

The shrinkage is one of the most important defect of agricultural drying products which major effect to the market value. This defect related to appearance, texture, and size change of dried food materials. The shrinkage is usually occurred during the hot-air drying due to the moisture loss and heating that causes the stress in its cellular structure [5-6]. The research reported that dried kiwifruit had shrunk to 81.76% of its original volume. In addition, its shrinkage behavior during hot-air drying was similar to the pattern of drying curve. In the early stages of the drying, the volume of kiwifruit decreased highly and then decreased towards the end of the process gradually [7]. However, the hot-air drying of ripe mangoes [8] and pears [9] indicated that the shrinkage of their slices increased linearly with decrease in moisture content and found that the air temperature had less influence on their shrinkage. Moreover, Ratti [10] also demonstrated that the shrinkage of potatoes, apples, and carrots was independent of air temperature and relative humidity while the air velocity had less effect on shrinkage of apples and carrots. On the other hand, some study found that the higher air temperatures and air velocities provided lower shrinkage, for instance, in dried hawthorn fruits [11]. However, there has never been any research about the shrinkage of ripe mango in both of swirling and non-swirling air flow drying process.

There were some research that reported shrinkage by taking the samples out of the drying process in order to measure their size [7-11]. Unfortunately, this way is not appropriate methodology because an equilibrium of heat and mass transfer of the drying process in chamber are disturbed. Accordingly, it resulted in errors and uncertainties of experiments [12]. To solve this problem, the computer vision system (CVS) should be applied for area measurement throughout

the drying process. The advantages of CVS are non-invasive, objective results, fast, real-time monitoring that makes the necessary results, non-destructive analysis and cost saving [12-13]. The main compositions of CVS were digital or video camera(s), illuminants, and computer software [13]. The previous literatures showed that the CVS was able to measure the color change and the area of food which is related to shrinkage, during the drying process [14-16]. Therefore, the aims of this work were to study the effect of swirling and non-swirling air flow on drying kinetics of ripe mango and to investigate the area shrinkage of ripe mango during the drying process by CVS.

Materials and Methods

Sample Preparation

Ripe mango, *Mangifera indica* cv. 'Nam Dok Mai Si Thong' was purchased from a local market in Nakhon Pathom (Thailand). The total soluble solids (TSS), titratable acidity (TA), and penetration resistance of the samples were used as the criteria parameters for sample selection. The TSS and penetration resistance were measured by a refractometer (Optika HR-130, Italy) and penetrometer (FT 327, Italy), respectively. The TA was estimated by titration method as described by Sogi et al. [17]. For our experiment, the TSS, TA, and penetration resistance of selected samples were $18.32 \pm 1.02^\circ$ Brix, 0.32 ± 0.06 g citric acid/100 g sample, and 12.76 ± 2.52 N, respectively. The initial moisture content of selected sample was determined by standard method [18], which was 469 ± 0.34 % (dry basis). The selected samples were cut into a slab shape with 1.0 cm thickness, 1.5 cm width, and 1.5 cm length.

Experimental Setup

Swirling and non-swirling air flow dryers were used as previously described by Malaikritsanachalee et al. [2]. In addition, both of that dryers were modified for investigation of sample size area during the drying process by using CVS. The schematic diagram of the dryer was shown in Figure 1. The constituents of CVS are a digital camera, illuminants, computer software and computer hardware. Images were obtained from the digital camera module (CMOS digital image sensor IMX179, SONY, Japan) with a resolution of 3264×2448 pixels. The camera was placed 30 cm above center of the tray. Four illuminants (LED, Daylight 6500 K,120° viewing angle, SMDS 5050, Epistar, Taiwan) were placed on chamber wall above the sample plane of 10 cm and of 45o angle as shown in Figure 1. The developed software using Visual Basic (VB) language was applied to interface the digital camera with a PC. The sample images were captured and then transferred to PC. Finally, the sample area shrinkage was analyzed in the same sampling interval according to setting measurement described in drying procedures below.
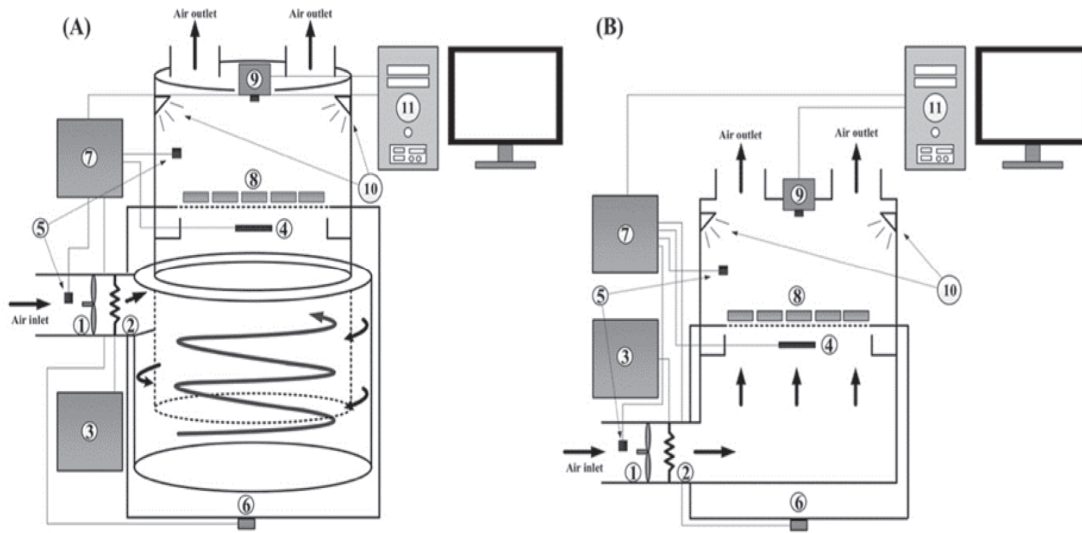
Figure 1 The experimental setup of (A) swirling flow dryer and (B) non-swirling flow dryer was comprised (1) fan, (2) heater, (3) temperature controller, (4) PT100 temperature sensor, (5) temperature and humidity sensors, (6) load cell, (7) data loggers, (8) single layer tray, (9) digital camera, (10) illuminants, (11) Computer

Drying Procedures

The initial weight of selected sample was 4.70 ± 0.45 g. The samples were placed on tray and then put into the drying chamber after the drying temperature reached to steady state. The samples were dried at 50, 60, and 70°C air temperatures and 1.0, 1.5, and 2.0 m/s air velocities for both swirling and non-swirling air flow until moisture content of the samples was reduced to 15.00% (dry basis) approximately. During the drying process, the sample weight, ambient temperature, inlet and outlet relative humidity, inlet and outlet air temperature were recorded every 1 minute by data logger (Lufft Opus 200).

Data Analysis of Drying Parameters

The drying curves were obtained from moisture ratio (Equation 1) and drying time. They were fitted with four different drying models as following; Lewis model in Equation 2 [19], Page model in Equation 3 [20], Henderson and Pabis model in Equation 4 [21] and Logarithmic model in Equation 5 [22].

$$MR = \frac{X_t\text{-}X_{eq}}{X_i\text{-}X_{eq}} \tag{1}$$

$$MR = \exp(-kt) \tag{2}$$

$$MR = \exp(-kt^n) \tag{3}$$

$$MR = a \cdot \exp(-kt) \tag{4}$$

$$MR = a \cdot \exp(-kt) + c \tag{5}$$

Where MR is moisture ratio (-), X_i is initial moisture content (kg water·kg dry matter^{-1}), X_t is moisture content at any time (kg water·kg dry matter^{-1}), X_{eq} is equilibrium moisture content (kg water·kg dry matter^{-1}), t is drying time (s) and a, c, k and n are model constants.

Non-linear regression analysis was performed by using open source software on R platform to evaluate the model constants. The goodness of fit model could be illustrated by three parameters; coefficient of determination (R^2), the reduced chi-square (X^2), and the root mean square error (RMSE) as shown in Equation 6, 7, and 8, respectively.

$$R^2 = 1 - \frac{\text{Residual sum square}}{\text{Total sum square}} \tag{6}$$

$$\chi^2 = \frac{\sum_{i=1}^{n}\left[MR_{exp,i} - MR_{pre,i}\right]^2}{n - z} \tag{7}$$

$$RMSE = \left(\frac{1}{n}\sum_{i=1}^{n}\left[MR_{exp,i} - MR_{pre,i}\right]^2\right)^{1/2} \tag{8}$$

Where MR_{exp} is experimental moisture ratio (-), MR_{pre} is predicted moisture ratio (-), n is number of observations and z is number of constants in the drying model.

In order to estimate the rate of moisture loss during the drying process, the drying rates (DR) were determined from the changes of moisture content in the samples per each unit of time as shown in Equation 9.

$$DR = -\frac{X_{t+\Delta t} - X_t}{\Delta t} \tag{9}$$

Where DR is drying rate (kg water·kg dry matter^{-1} s^{-1}), $X_t + \Delta_t$ is moisture content at $t + \Delta t$ (kg water·kg dry matter^{-1}) and Δt is time increment (s).

The ripe mangoes were cut into a dimension of 1.0 cm thickness×1.5 cm width×1.5 cm length that was considered as three-dimensional moisture transfer. Thus, the diffusion model based on the Fick's second law of diffusion in Equation 10 was used to determine the effective moisture diffusivity (D_{eff}) and to describe the moisture transport from ripe mangoes [23-24]. The assumptions of this model in our experiment are uniform initial moisture content, non-shrinking slab, and constant D_{eff} throughout the sample.

$$MR = \frac{8^3}{\pi^6} \sum_{n=0}^{\infty} \sum_{m=0}^{\infty} \sum_{k=0}^{\infty} \frac{1}{(2n+1)^2 (2m+1)^2 (2k+1)^2}$$

$$\times \exp\left[-(2n+1)^2 \frac{\pi^2 D_{eff}}{4X^2} t\right]$$

$$\times \exp\left[-(2m+1)^2 \frac{\pi^2 D_{eff}}{4Y^2} t\right] \tag{10}$$

$$\times \exp\left[-(2k+1)^2 \frac{\pi^2 D_{eff}}{4Z^2} t\right]$$

Where X, Y, and Z are half thickness of the samples (m) in the width, length, and thickness, respectively, D_{eff} is effective moisture diffusivity (m^2/s) and n, m, and k are indexes of summations.

For a long drying time, Equation 10 was able to simplify by neglect all other terms of the series. Additionally, sample width, length, and thickness must be considered as a function of time in order to consider the shrinkage effect. The sample shrinkage was assumed to be a symmetric shrinkage. Consequently, Equation 10 became [8, 23]:

$$MR = \frac{8^3}{\pi^6} \exp\left(-\frac{\pi^2 D_{eff}}{4L_t^2} t\right) \tag{11}$$

Where $L_t^2 = X_t^2 + Y_t^2 + Z_t^2$. X_t, Y_t, and Z_t are half thickness of the samples at any time (m) in width, length, and thickness, respectively.

Thus, ln(MR) from the best drying model versus t/L_t^2 was plotted to determine the slope that related to constant D_{eff} as shown in Equation 12.

$$\text{Slope} = \frac{\pi^2 D_{eff}}{4} \tag{12}$$

Area Shrinkage Measurement

The CVS was applied to measure and investigate a sample area shrinkage during the drying process. The sample area shrinkage was determined by pixels counting from sample image. By CVS measurement, the sample images were captured and saved in JPEG format. Each piece of the sample images was segmented by using a thresholding-based method [25]. The pixel numbers of segmented images were determined.

The pixels were converted into square meters (m^2) by calibration method using standard images. The five sizes of white square images (0.5×0.5, 1.0×1.0, 1.5×1.5, 2.0×2.0 and 2.5×2.5 cm) on the black background were used to be standard images. They were drawn

by computer aided design (CAD) software and printed by a printer (Fuji Xerox DocuPrint C2200, Japan). Standard images were placed and captured at the same position on the tray. The pixel numbers of white square shape were examined. This procedure was conducted for all standard images in three replicates. A regression model was found from calibration curve of the pixel number and their corresponding sizes as shown in Equation 13. This calibration method was adapted from Sampson et al. [15].

$$A = (6.8150 \times 10^{-9}) \times N \qquad (13)$$

Where A is area of the sample (m^2) and N is pixel number of the sample area.

For sample area measurement, the pixel numbers were converted to the area by regression model in Equation 13. Therefore, the area shrinkage of the samples could be calculated by using Equation 14.

$$S = \frac{A_i - A_t}{A_i} \times 100\% \qquad (14)$$

Where S is area shrinkage percentage (%), Ai is initial area of the sample (m^2) and A_t is area of the sample at any time (m^2)

Statistical Analysis

All experiments were performed in three replicates and reported as average values. One-way analysis of variance (one-way ANOVA) was used to assess the effect of drying conditions on D_{eff} and S by SPSS software v.18. The multiple comparisons of significant treatment were performed by using Duncan's multiple range test at $p < 0.05$ significance level and 95% confidence interval.

Results and Discussion

Kinetics Modeling of Experiment

To assign the appropriate kinetic modeling of our experiment, the drying curves at different conditions were fitted with four drying models. Indications of appropriate model are higher R^2 values, lower RMSE, and χ^2 values as shown in Table 1. The results showed that the highest R^2 values (0.9826-0.9990), the lowest RMSE (6.0732×10^{-3}-3.4341×10^{-2}), and χ^2 (3.6962×10^{-5}-1.1850×10^{-3}) values were obtained from Page model. Therefore, Page model was most eligible to demonstrate drying behavior of ripe mangoes in swirling and non-swirling air flow drying. According to many previous studies, the results found that Page model was optimum fitting model for hot-air drying [8, 26-27] and solar drying [28] in mangoes.

Table 1 Fitting statistics of various drying models from swirling and non-swirling air flow drying at different conditions

Drying conditions	Model no.	Model constants	R^2	RMSE	χ^2
Swirling flow					
50°C and 1.0 m/s	1	k = 1.3368×10^{-4}	0.9957	1.4972×10^{-2}	2.2453×10^{-4}
	2	k = 1.3372×10^{-4}, n = 0.9999	**0.9959**	**1.4673×10^{-2}**	**2.1603×10^{-4}**
	3	a = 1.0005, k = 1.3388×10^{-4}	0.9957	1.4972×10^{-2}	2.2491×10^{-4}
	4	a = 0.9999, k = 1.3369×10^{-4}, c = 2.8819×10^{5}	0.9957	1.4972×10^{-2}	2.2530×10^{-4}
50°C and 1.5 m/s	1	k = 1.3782×10^{-4}	0.9990	6.0734×10^{-3}	3.7035×10^{-5}
	2	k = 1.3832×10^{-4}, n = 0.9996	**0.9990**	**6.0732×10^{-3}**	**3.6962×10^{-5}**
	3	a = 1.0553, k = 1.5985×10^{-4}	0.9858	2.2878×10^{-2}	5.2552×10^{-4}
	4	a = 1.0000, k = 1.3783×10^{-4}, c = 3.9737×10^{-5}	0.9990	6.0734×10^{-3}	3.7113×10^{-5}
50°C and 2.0 m/s	1	k = 1.5404×10^{-4}	0.9955	1.6544×10^{-2}	2.7423×10^{-4}
	2	k = 1.7561×10^{-4}, n = 0.9855	**0.9956**	**1.6414×10^{-2}**	**2.7043×10^{-4}**
	3	a = 1.0000, k = 1.5404×10^{-4}	0.9955	1.6544×10^{-2}	2.7473×10^{-4}
	4	a = 1.0000, k = 1.5423×10^{-4}, c = 3.2848×10^{-4}	0.9955	1.6545×10^{-2}	2.7527×10^{-4}
60°C and 1.0 m/s	1	k = 1.5290×10^{-4}	0.9958	1.6205×10^{-2}	2.6313×10^{-4}
	2	k = 2.0961×10^{-4}, n = 0.9650	**0.9963**	**1.5318×10^{-2}**	**2.3557×10^{-4}**
	3	a = 1.0000, k = 1.5290×10^{-4}	0.9958	1.6205×10^{-2}	2.6365×10^{-4}
	4	a = 1.0000, k = 1.5293×10^{-4}, c = 5.5084×10^{-5}	0.9958	1.6205×10^{-2}	2.6417×10^{-4}
60°C and 1.5 m/s	1	k = 1.7994×10^{-4}	0.9989	8.5520×10^{-3}	7.3331×10^{-5}
	2	k = 2.0605×10^{-4}, n = 0.9847	**0.9990**	**8.2149×10^{-3}**	**6.7845×10^{-5}**
	3	a = 1.0000, k = 1.7994×10^{-4}	0.9989	8.5520×10^{-3}	7.3527×10^{-5}
	4	a = 1.0000, k = 1.7986×10^{-4}, c = -1.2954×10^{-4}	0.9989	8.5521×10^{-3}	7.3727×10^{-5}
60°C and 2.0 m/s	1	k = 2.1872×10^{-4}	0.9941	1.8906×10^{-2}	3.5835×10^{-4}
	2	k = 3.3323×10^{-4}, n = 0.9515	**0.9949**	**1.7538×10^{-2}**	3.0913×10^{-4}
	3	a = 1.0000, k = 2.1872×10^{-4}	0.9941	1.8906×10^{-2}	3.5925×10^{-4}
	4	a = 0.9999, k = 2.1879×10^{-4}, c = 8.6432×10^{-5}	0.9941	1.8906×10^{-2}	3.6016×10^{-4}
70°C and 1.0 m/s	1	k = 2.2778×10^{-4}	0.9963	1.2472×10^{-2}	1.5596×10^{-4}
	2	k = 2.8606×10^{-4}, n = 0.9734	**0.9966**	**1.1979×10^{-2}**	**1.4424×10^{-4}**
	3	a = 1.0069, k = 2.3159×10^{-4}	0.9961	1.2718×10^{-2}	1.6258×10^{-4}
	4	a = 0.9999, k = 2.2974×10^{-4}, c = 2.1656×10^{-4}	0.9963	1.2473×10^{-2}	1.5677×10^{-4}

Table 1 (continued) Fitting statistics of various drying models from swirling and non-swirling air flow drying at different conditions

Drying conditions	Model no.	Model constants	R^2	RMSE	χ^2
70°C and 1.5 m/s	1	$k = 2.4257 \times 10^{-4}$	0.9944	1.7757×10^{-2}	3.1608×10^{-4}
	2	$k = 3.4236 \times 10^{-4}$, n = 0.9598	**0.9949**	$\mathbf{1.6902 \times 10^{-2}}$	$\mathbf{2.8704 \times 10^{-4}}$
	3	a = 1.0000, $k = 2.4257 \times 10^{-4}$	0.9944	1.7757×10^{-2}	3.1683×10^{-4}
	4	a = 0.9999, $k = 2.4246 \times 10^{-4}$, $c = -1.1873 \times 10^{-4}$	0.9944	1.7758×10^{-2}	3.1759×10^{-4}
70°C and 2.0 m/s	1	$k = 2.7174 \times 10^{-4}$	0.9972	1.2366×10^{-2}	1.5344×10^{-4}
	2	$k = 2.9647 \times 10^{-4}$, n = 0.9894	0.9972	$\mathbf{1.2301 \times 10^{-2}}$	$\mathbf{1.5238 \times 10^{-4}}$
	3	a = 1.0409, $k = 3.0335 \times 10^{-4}$	0.9925	2.0141×10^{-2}	4.0851×10^{-4}
	4	a = 1.0000, $k = 2.7176 \times 10^{-4}$, $c = 2.0175 \times 10^{-5}$	0.9972	1.2366×10^{-2}	1.5452×10^{-4}
Non-Swirling flow					
50°C and 1.0 m/s	1	$k = 1.1460 \times 10^{-4}$	0.9965	1.3997×10^{-2}	1.9628×10^{-4}
	2	$k = 1.5733 \times 10^{-4}$, n = 0.9652	**0.9969**	$\mathbf{1.3179 \times 10^{-2}}$	$\mathbf{1.7431 \times 10^{-4}}$
	3	a = 1.0557, $k = 1.3332 \times 10^{-4}$	0.9871	2.6855×10^{-2}	7.2379×10^{-4}
	4	a = 1.0001, $k = 1.1449 \times 10^{-4}$, $c = -3.2944 \times 10^{-4}$	0.9965	1.3998×10^{-2}	1.9700×10^{-4}
50°C and 1.5 m/s	1	$k = 1.2376 \times 10^{-4}$	0.9986	7.4297×10^{-3}	5.5301×10^{-5}
	2	$k = 1.3900 \times 10^{-4}$, n = 0.9872	0.9986	7.2440×10^{-3}	5.2667×10^{-5}
	3	a = 1.0259, $k = 1.3212 \times 10^{-4}$	0.9956	1.2915×10^{-2}	1.6740×10^{-4}
	4	a = 1.0002, $k = 1.2363 \times 10^{-4}$, $c = -4.1244 \times 10^{-4}$	0.9986	7.4299×10^{-3}	5.5506×10^{-5}
50°C and 2.0 m/s	1	$k = 1.3077 \times 10^{-4}$	0.9941	1.9007×10^{-2}	3.6250×10^{-4}
	2	$k = 1.2915 \times 10^{-4}$, n = 1.0014	0.9941	1.9006×10^{-2}	3.6190×10^{-4}
	3	a = 1.0033, $k = 1.3189 \times 10^{-4}$	0.9940	1.9061×10^{-2}	3.6461×10^{-4}
	4	a = 0.9999, $k = 1.3092 \times 10^{-4}$, $c = 3.3948 \times 10^{-4}$	0.9941	1.9008×10^{-2}	3.6320×10^{-4}
60°C and 1.0 m/s	1	$k = 1.3619 \times 10^{-4}$	0.9820	3.4955×10^{-2}	1.2248×10^{-3}
	2	$k = 1.3917 \times 10^{-4}$, n = 0.9975	0.9826	3.4341×10^{-2}	1.1850×10^{-3}
	3	a = 0.9999, $k = 1.8045 \times 10^{-4}$	0.9820	3.4955×10^{-2}	1.2277×10^{-3}
	4	a = 1.0004, $k = 1.3598 \times 10^{-4}$, $c = -6.8402 \times 10^{-4}$	0.9820	3.4955×10^{-2}	1.2306×10^{-3}
60°C and 1.5 m/s	1	$k = 1.6215 \times 10^{-4}$	0.9949	1.7285×10^{-2}	2.9953×10^{-4}
	2	$k = 2.1753 \times 10^{-4}$, n = 0.9671	0.9953	1.6507×10^{-2}	2.7385×10^{-4}
	3	a = 1.0041, $k = 1.6375 \times 10^{-4}$	0.9948	1.7370×10^{-2}	3.0323×10^{-4}
	4	a = 1.0000, $k = 1.6208 \times 10^{-4}$, $c = -1.3405 \times 10^{-4}$	0.9949	1.7286×10^{-2}	3.0104×10^{-4}

Table 1   (continued) Fitting statistics of various drying models from swirling and non-swirling
air flow drying at different conditions

Drying conditions	Model no.	Model constants	R^2	RMSE	χ^2
60°C and 2.0 m/s	1	$k = 1.8577 \times 10^{-4}$	0.9976	1.0516×10^{-2}	1.1080×10^{-4}
	2	$k = 2.2935 \times 10^{-4}$, n = 0.9758	0.9978	1.0138×10^{-2}	1.0317×10^{-4}
	3	a = 1.0153, $k = 1.9292 \times 10^{-4}$	0.9970	1.1711×10^{-2}	1.3768×10^{-4}
	4	a = 1.0001, $k = 1.8557 \times 10^{-4}$, $c = -3.5578 \times 10^{-4}$	0.9976	1.0517×10^{-2}	1.1124×10^{-4}
70°C and 1.0 m/s	1	$k = 1.6322 \times 10^{-4}$	0.9892	2.4408×10^{-2}	5.9819×10^{-4}
	2	$k = 1.7008 \times 10^{-4}$, n = 0.9954	0.9892	2.4400×10^{-2}	5.9719×10^{-4}
	3	a = 1.0178, $k = 1.7243 \times 10^{-4}$	0.9876	2.6188×10^{-2}	6.8908×10^{-4}
	4	a = 1.0000, $k = 1.6320 \times 10^{-4}$, $c = -4.7065 \times 10^{-5}$	0.9892	2.4408×10^{-2}	6.0004×10^{-4}
70°C and 1.5 m/s	1	$k = 1.8835 \times 10^{-4}$	0.9976	1.2116×10^{-2}	1.4713×10^{-4}
	2	$k = 2.4783 \times 10^{-4}$, n = 0.9689	0.9979	1.1236×10^{-2}	1.2681×10^{-4}
	3	a = 1.0000, $k = 1.8835 \times 10^{-4}$	0.9976	1.2116×10^{-2}	1.4746×10^{-4}
	4	a = 0.9999, $k = 1.8872 \times 10^{-4}$, $c = 5.1905 \times 10^{-3}$	0.9976	1.2119×10^{-2}	1.4786×10^{-4}
70°C and 2.0 m/s	1	$k = 2.0773 \times 10^{-4}$	0.9891	2.4450×10^{-2}	5.9904×10^{-4}
	2	$k = 1.6645 \times 10^{-4}$, n = 1.0147	0.9891	2.4394×10^{-2}	5.9753×10^{-4}
	3	a = 1.0642, $k = 2.2904 \times 10^{-4}$	0.9778	3.4901×10^{-2}	1.2231×10^{-3}
	4	a = 1.0001, $k = 1.8881 \times 10^{-4}$, $c = -3.2705 \times 10^{-4}$	0.9891	2.4450×10^{-2}	6.0157×10^{-4}

Effect of Air Temperature and Air Velocity on Drying Behavior

Effect of air temperature, air velocity and air flow characteristic on drying behavior of ripe mangoes was illustrated in Figure 2A-C. The results showed that MR was exponential decay with drying time in all drying conditions. Moreover, the drying time decreased with increasing air temperature and air velocity. The drying time of swirling and non-swirling air flow drying process decreased to 52 and 45%, respectively when the air temperature increased from 50 to 70°C at the constant air velocity of 2.0 m/s. Likewise, the drying time of them could be reduced to 34% (in swirling flow) and 24% (in non-swirling flow) by increasing air velocity from 1.0 to 2.0 m/s at a constant air temperature of 60°C. The high air temperature and high air velocity provided the higher vapor pressure gradients between the ripe mangoes and the hot air, which led to an increase in rate of the moisture removal [26, 29, 30].

Effect of Flow Characteristic on Drying Behavior

The drying behavior of swirling air flow drying was similar to non-swirling air flow drying as shown in Figure 2A-C. Additionally, the swirling air flow application was able to reduce the drying time approximately 11−23% when compared with non-swirling air flow at the same condition. The shortest drying time was obtained from swirling air flow drying at 70°C air temperature and 2.0 m/s air velocity. This result indicated that heat and mass transfer definitely increased by using the swirling air flow because it generated small eddies when the air flowed through the tray. The small eddies flowed around the horizontal sample surface that disturbed the sample vapor density and caused the increase in sample surface temperature [31]. Consequently, the reduction of vapor density enhanced mass transfer between the sample and hot air [31-32] while the increasing of the sample surface temperature provided the higher water evaporation rate [11, 33].

Drying Rate

Figure 2D-F represented the drying rate of ripe mangoes at various conditions. The results showed that the drying rate linearly decreased when the moisture content (X/X_0) decreased in all drying conditions. This result was due to the decrease in moisture content could generate the vigorous bond between water and food components in ripe mangoes [34]. Furthermore, our experiment only found the falling rate period as the same in previous research [8, 28]. Due to the high sugar content of ripe mango, there was no free water in the sample, so a constant rate period was not present.

Effective Moisture Diffusivity

Table 2 demonstrated the effective moisture diffusivity (D_{eff}) of ripe mangoes drying at various conditions. The D_{eff} was used to describe the moisture transport from the samples and drying capability of the dryers. The D_{eff} of swirling air flow drying was in the range of $(4.48\text{-}9.71)\times10^{-9}$ m^2/s, while the D_{eff} of non-swirling air flow drying was in the range of $(3.41\text{-}7.24)\times10^{-9}$ m^2/s. In addition, effect of air velocity and air temperature on the D_{eff} of swirling and non-swirling air flow drying was represented as a contour plot in Figure 3A and B, respectively. The results indicated that the D_{eff} increased with increasing air temperature and air velocity for both swirling and non-swirling air flow drying. Furthermore, the D_{eff} of swirling air flow drying was more enhanced than that of non-swirling air flow drying. It could be concluded that the swirling air flow promoted the synergistic effect of air temperature and air velocity on the drying by disturbance the boundary of air layer on the sample surface [2].
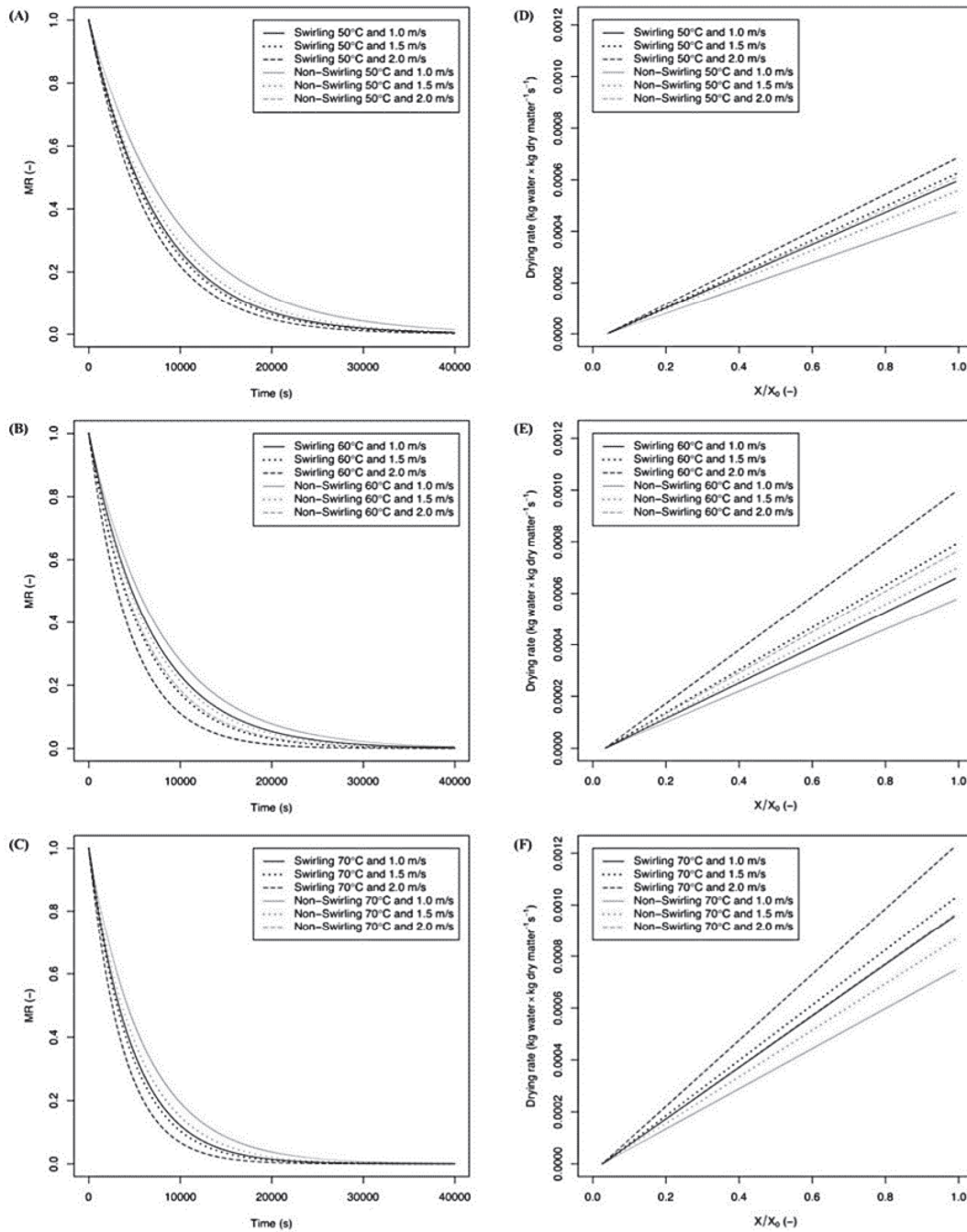
Figure 2 Drying curves (A–C) and drying rate (D–F) of ripe mangoes from swirling and non-swirling air flow drying at various conditions

Table 2 Effective diffusivity coefficient (Deff) and area shrinkage percentage (S) of dried ripe mangoes from swirling and non-swirling air flow drying at various conditions

Drying conditions	D_{eff} (m²/s)×10⁹	S (%)
Swirling flow		
50°C and 1.0 m/s	4.70 ± 0.10^{fg}	34.92 ± 3.38^{ef}
50°C and 1.5 m/s	4.48 ± 0.15^{g}	40.98 ± 2.90^{abcd}
50°C and 2.0 m/s	5.22 ± 0.25^{de}	37.38 ± 2.61^{cdef}
60°C and 1.0 m/s	5.00 ± 0.07^{ef}	38.01 ± 3.85^{bcdef}
60°C and 1.5 m/s	5.71 ± 0.22^{c}	40.35 ± 2.60^{abcde}
60°C and 2.0 m/s	7.63 ± 0.55^{b}	36.58 ± 2.53^{def}
70°C and 1.0 m/s	7.64 ± 0.42^{b}	32.64 ± 3.30^{f}
70°C and 1.5 m/s	7.55 ± 0.06^{b}	37.73 ± 3.63^{bcdef}
70°C and 2.0 m/s	9.71 ± 0.14^{a}	33.56 ± 4.97^{f}
Non-Swirling flow		
50°C and 1.0 m/s	3.41 ± 0.10^{h}	40.63 ± 2.16^{abcd}
50°C and 1.5 m/s	3.80 ± 0.07^{h}	43.44 ± 2.96^{a}
50°C and 2.0 m/s	4.48 ± 0.08^{g}	39.41 ± 2.95^{abcde}
60°C and 1.0 m/s	4.27 ± 0.44^{g}	38.04 ± 2.97^{abcdef}
60°C and 1.5 m/s	4.74 ± 0.10^{efg}	42.96 ± 3.01^{ab}
60°C and 2.0 m/s	5.56 ± 0.17^{cd}	39.46 ± 3.30^{abcde}
70°C and 1.0 m/s	5.83 ± 0.17^{c}	36.45 ± 4.93^{def}
70°C and 1.5 m/s	5.91 ± 0.44^{c}	42.76 ± 3.09^{abc}
70°C and 2.0 m/s	7.24 ± 0.41^{b}	37.97 ± 3.28^{bcdef}

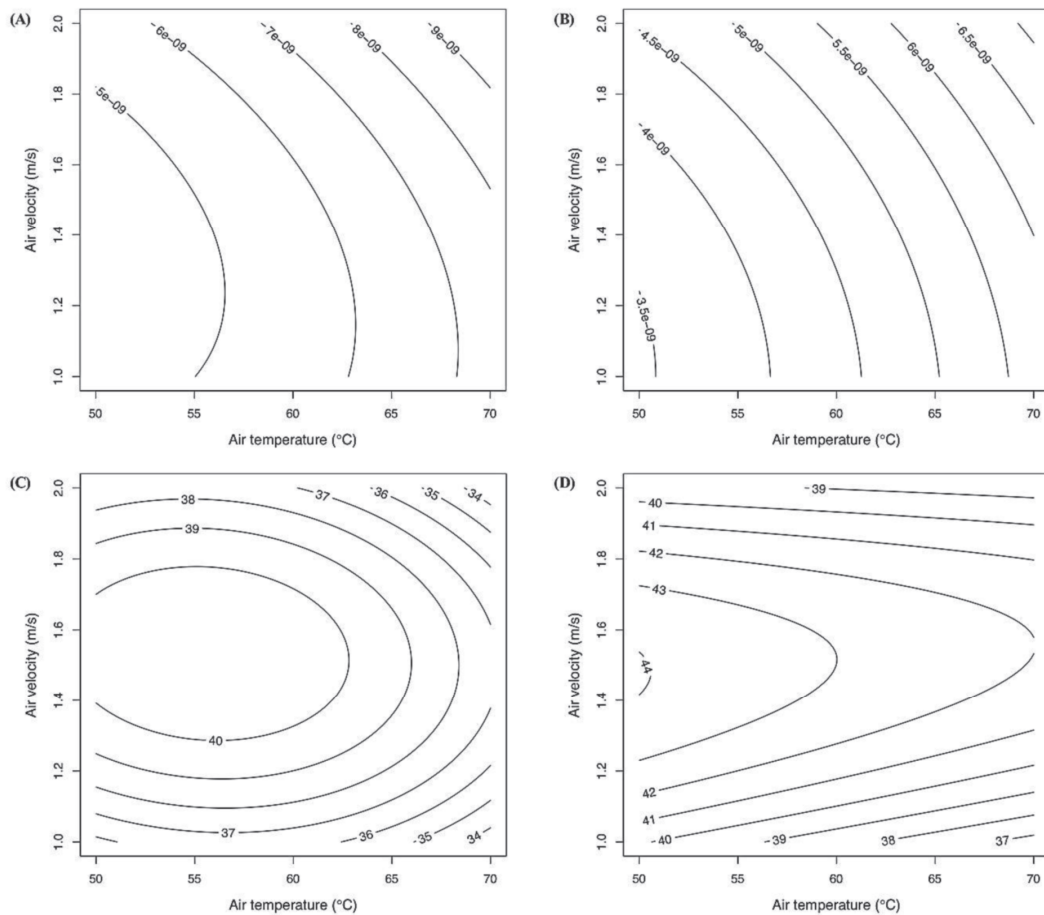[a-h]Different letters in the same column indicate significant differences (P<0.05).

Figure 3 Effect of air velocity and air temperature on the effective diffusivity coefficient (D$_{eff}$) of (A) swirling and (B) non-swirling air flow drying and the area shrinkage percentage (S) of dried ripe mangoes from (C) swirling and (D) non-swirling air flow drying

Shrinkage Behavior of Ripe Mangoes

As shown in Table 2, the area shrinkage represented the percentage changes of the sample surface area at the moisture content of 15.00% (dry basis). The area shrinkage of swirling air flow drying was in the range of 32.64-40.98% while the area shrinkage of non-swirling air flow drying was in the range of 36.45-43.44%. The results indicated that the application of swirling air flow was able to reduce the area shrinkage of dried ripe mangoes. Moreover, the area shrinkage decreased with increasing air temperature when compared with the same air velocity for both swirling and non-swirling air flow drying. This result was due to the rigid crust or case hardening might be formed on the sample surface by increase in drying rate [1, 5, 10-11]
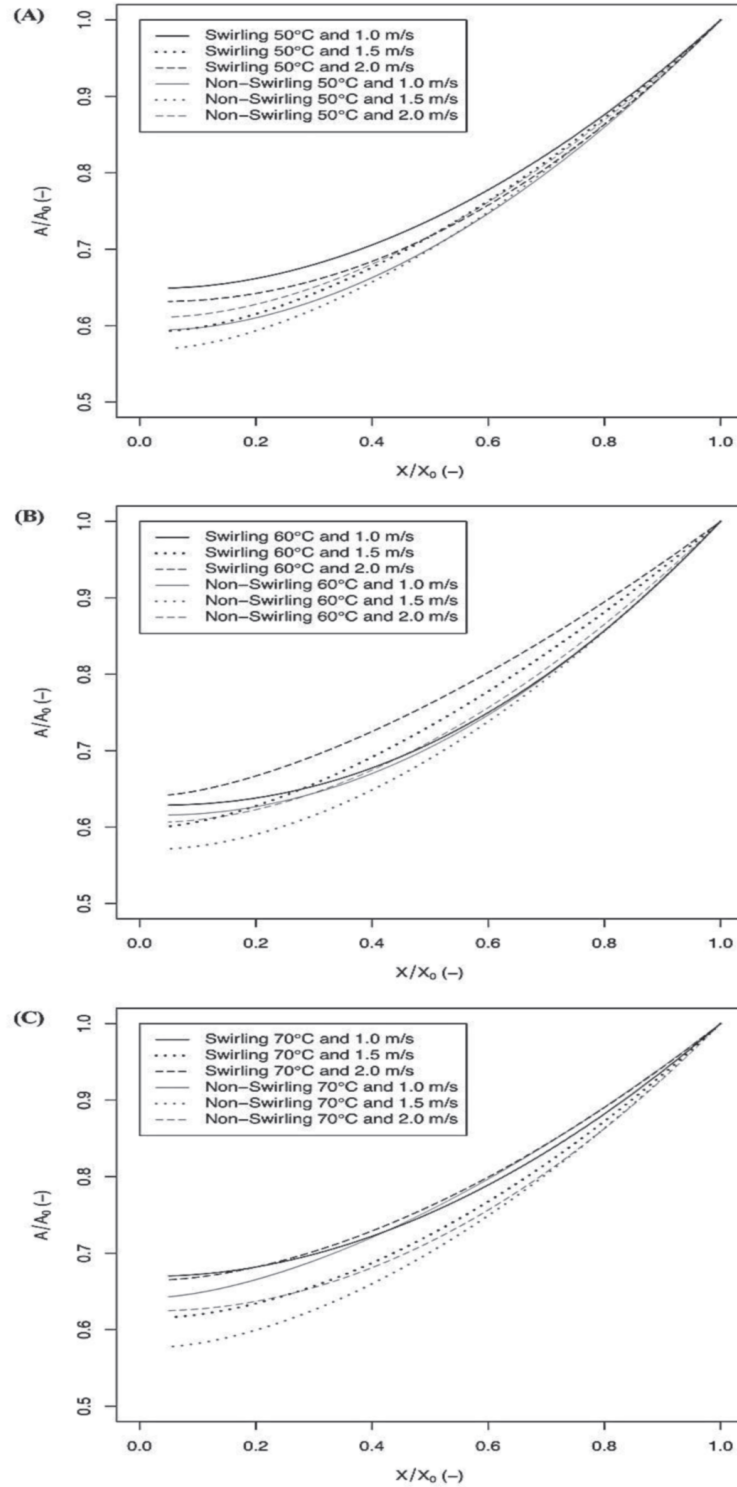
Figure 4 Area shrinkage as a function of their moisture content for swirling and non-swirling air flow drying at (A) 50 °C, (B) 60 °C, (C) 70 °C

Figure 4A-C illustrated the shrinkage mechanism of ripe mangoes in drying process at various conditions by the area ratio with moisture content. At high moisture content, the sample was fully occurred in the rubbery state. Accordingly, the sample area was linearly decreased with decreasing moisture content. At low moisture content, the samples became more viscous and then, rigidity of the sample increased. Consequently, the shrinkage of sample area occurred slowly by increase in rigidity of the sample structure that was the result from the enlargement of glass transition temperature of the sample [5-6].

Moreover, Figure 3C and D also demonstrated the effect of air velocity and air temperature on the area shrinkage percentage of dried ripe mangoes from swirling and non-swirling air flow drying, respectively. The results showed that, the area shrinkage was highest at constant air velocity of 1.5 m/s when compared with the same air temperature for both swirling and non-swirling air flow drying. The shrinkage phenomenon from the results in Figure 4A-C clearly indicated that the area ratio of the sample with air velocity of 1.5 m/s at lower moisture content was more rapidly decreased than that of the other value of air velocity. These results were because of the internal stress of materials and case hardening formation. For the lower air velocity (1.0 m/s), the moisture gradient between inner and surface of materials was small that led to low internal stress and caused gradually slow shrinkage. For the higher air velocity (1.5 m/s), the moisture gradient was more increased that resulted in the shrinkage rather than that at the lower air velocity. For the highest air velocity (2.0 m/s), the moisture gradient was large, whereas the moisture content at the sample surface rapidly decreased and then caused the formation of case hardening [10-11]. Therefore, the area shrinkage at 2.0 m/s air velocity was lower than that at 1.5 m/s air velocity.

Conclusions

In this study, the effect of swirling and non-swirling air flow on drying kinetics and area shrinkage of ripe mangoes were determined. The results were concluded that Page model showed to be the best fitting model to represent the drying behaviors of ripe mangoes. The D_{eff} decreased when the air temperature and air velocity increased for both swirling and non-swirling air flow drying, whereas the area shrinkage decreased with increasing air temperature for both of them. The area shrinkage behavior related to moisture content was similar to the pattern of drying curve, which decreased as an exponential decay. Furthermore, the application of swirling air flow was able to reduce the drying time and area shrinkage of dried ripe mangoes.

Acknowledgements

References

1. Wang, J., Law, C. L., Nema, P. K., Zhao, J. H., Liu, Z. L., Deng, L. Z., Gao, Z. J., & Xiao, H. W. (2018). Pulsed vacuum drying enhances drying kinetics and quality of lemon slices. *Journal of Food Engineering, 224,* 129-138.

2. Malaikritsanachalee, P., Choosri, W., & Choosri, T. (2018). Study on kinetics of flow characteristics in hot air drying of pineapple. *Food Science and Biotechnology, 27*(4), 1047-1055.

3. Çakmak, G., & Yildiz, C. (2009). Design of a new solar dryer system with swirling flow for drying seeded grape. *International Communications in Heat and Mass Transfer, 36*(9), 984-990.

4. Özbey, M., & Söylemez, M. S. (2005). Effect of swirling flow on fluidized bed drying of wheat grains. *Energy Conversion and Management, 46*(9-10), 1495-1512.

5. Mayor, L., & Sereno, A. M. (2004). Modelling shrinkage during convective drying of food materials: A review. *Journal of Food Engineering, 61*(3), 373-386.

6. Sappati, P. K., Nayak, B., & Walsum, G. P. V. (2017). Effect of glass transition on the shrinkage of sugar kelp (*Saccharina latissima*) during hot air convective drying. *Journal of Food Engineering, 210,* 50-61.

7. Maskan, M. (2001). Drying, shrinkage and rehydration characteristics of kiwifruits during hot air and microwave drying. *Journal of Food Engineering, 48*(2), 177-182.

8. Dissa, A. O., Desmorieux, H., Bathiebo, J., & Koulidiati, J. (2008). Convective drying characteristics of Amelie mango (*Mangifera Indica* L. cv. 'Amelie') with correction for shrinkage. *Journal of Food Engineering, 88*(4), 429-437.

9. Mrad, D. N., Boudhrioua, N., Kechaou, N., Courtois, F., & Bonazzi, C. (2012). Influence of air drying temperature on kinetics, physicochemical properties, total phenolic content and ascorbic acid of pears. *Food and Bioproducts Processing, 90*(3), 433-441.

10. Ratti, C. (1994). Shrinkage during drying of foodstuffs. *Journal of Food Engineering, 23*(1), 91-105.

11. Aral, S., & Başe, A. V. (2016). Convective drying of hawthorn fruit (*Crataegus* spp.): Effect of experimental parameters on drying kinetics, color, shrinkage, and rehydration capacity. *Food Chemistry, 210,* 577-584.

12. Hosseinpour, S., Rafiee, S., Mohtasebi, S. S., & Aghbashlo, M. (2013). Application of computer vision technique for on-line monitoring of shrimp color changes during drying. *Journal of Food Engineering, 115*(1), 99-114.

13. Brosnan, T., & Sun, D. W. (2004). Improving quality inspection of food products by computer-vision: a review. *Journal of Food Engineering, 61*(1), 3-16.

14. Sturm, B., Hofacker, W. C., & Hensel, O. (2012). Optimizing the Drying Parameters for Hot-Air−Dried Apples. *Drying Technology, 30*(14), 1570-1582.

15. Sampson, D. J., Chang, Y. K., Rupasinghe, H. P. V., & Zaman, Q. U. Z. (2014). A dual-view computer-vision system for volume and image texture analysis in multiple apple slices drying. *Journal of Food Engineering, 127,* 49-57.

16. Nadian, M. H., Abbaspour-Fard, M. H., Martynenko, A., & Golzarian, M. R. (2017). An intelligent integrated control of hybrid hot air-infrared dryer based on fuzzy logic and computer vision system. *Computers and Electronics in Agriculture, 137,* 138-149.

17. Sogi, D. S., Siddiq, M., & Dolan, K. D. (2015). Total phenolics, carotenoids and antioxidant properties of Tommy Atkin mango cubes as affected by drying techniques. *LWT−Food Science and Technology, 62*(1), 564-568.

18. AOAC. (2005). *Determination of Moisture, Ash, Protein and Fat. Official Method of Analysis of the Association of Analytical Chemists* (18th Edition). AOAC, Washington DC.

19. Lewis, W. K. (1921). The rate of drying solid materials. *Journal of Industrial and Engineering Chemistry, 13*(5), 427-432.

20. Lemus-Mondaca, R., Vega-Galvez, A., Moraga, N.O., & Astudillo, S. (2015). Dehydration of Stevia rebaudiana bertoni leaves: Kinetics, modeling and energy features. *Journal of Food Processing and Preservation, 39*(5), 508-520.

21. Henderson, S. M., & Pabis, S. (1961). Grain drying theory I: temperature effect on drying coefficient. *Journal of Agricultural Engineering Research, 6,* 169-174.

22. Yagcioglu, A., Degirmencioglu, A., & Cagatay, F. (1999). Drying characteristics of laurel leaves under different conditions. In A. Başçetinçelik (Ed.), *Proceedings of the 7th International Congress on Agricultural Mechanization and Energy* (pp. 565-569). Adana, Turkey. Faculty of Agriculture, Çukurova University.

23. Crank J. (1975). *The Mathematics of diffusion* (2nd ed., pp. 411). Clarendon Press, Oxford, UK.

24. Pasban, A., Sadrnia, H., Mohebbi, M., & Shahidi, S. A. (2017). Spectral method for simulating 3D heat and mass transfer during drying of apple slices. *Journal of Food Engineering, 212,* 201-212.

25. Otsu, N. (1979). A threshold selection method from gray-level histograms. *IEEE Transactions on Systems, Man, and Cybernetics, 9*(1), 62-66.

26. Goyal, R. K., Kingsly, A. R. P., Manikantan, M. R. ,& Ilyas, S. M. (2006). Thin-layer drying kinetics of raw mango slices. *Biosystems Engineering, 95*(1), 43-49.

27. Sehrawat, R., Nema, P. K., & Kaur, B. P. (2018). Quality evaluation and drying characteristics of mango cubes dried using low-pressure superheated steam, vacuum and hot air drying methods. *LWT Food Science and Technology, 92,* 548-555.

28. Wang, W., Li, M., Hassanien, R. H. E., Wang, Y., & Yang, L. (2018). Thermal performance of indirect forced convection solar dryer and kinetics analysis of mango. *Applied Thermal Engineering, 134,* 310-321.

29. Kha, T. C., Nguyen, M. H., Roach, P. D., & Stathopoulos, C. E. (2014). Microencapsulation of Gac oil: Optimisation of spray drying conditions using response surface methodology. *Powder technology. 264,* 298-309.

30. Zhu, A., & Shen, X. (2014). The model and mass transfer characteristics of convection drying of peach slices. *International Journal of Heat and Mass Transfer, 72,* 345-351.

31. Sedahmed, G. H., Abdel-Aziz, M. H., Abdo, M. S. E., Hassan, M. S., & Konsowa, A. H. (2017). Mass and heat transfer the surface of a gas sparged pool of liquid to an immiscible liquid under swirling flow and potential applications. *Chemical Engineering Research and Design, 125,* 88-95.

32. Javed, K. H., Mahmud, T., & Purba, E. (2006). Enhancement of mass transfer in a spray tower using swirling gas flow. *Chemical Engineering Research and Design, 84*(6), 465-477.

33. Tang, Y., Min, J., & Wu, X. (2018). Selection of convective moisture transfer driving potential and its impacts upon porous plate air-drying characteristics. *International Journal of Heat and Mass Transfer, 116,* 371-376.

34. Telis-Romero, J., Kohayakawa, M. N., Silveira, Jr. V., Pedro, M. A. M., & Gabas, A. L. (2005). Enthalpy-entropy compensation based on isotherms of mango. *Food Science and Technology, 25*(2), 297-303.